Preprints of the 21st IFAC World Congress (Virtual)
Berlin, Germany, July 12-17, 2020

Modeling and Voltage Control of Bidirectional Resonant DC/DC Converter for Application in Marine Power Systems

Martina Joševski * **Asimenia Korompili** * **Antonello Monti** *

* *E.ON Energy Research Center, Institute Automation of Complex Power Systems, RWTH Aachen University, Germany (e-mail: {martina.josevski,akorompili,amonti}@eonerc.rwth-aachen.de*

Abstract: DC/DC converters have gained popularity in a number of industrial applications like electric vehicles or marine power systems, due to their high efficiency and power density levels. Pulse width modulation (PWM) and resonant converters are two main types of the DC/DC converters. Thereby, the resonant converters happen to be the preferred technology in the design of modern marine power systems since these converters are more suitable for the high and middle voltage DC applications. The resonant converters are, however, highly nonlinear systems, which limits the use of linear control methods. In this study, we propose a comprehensive analysis, modeling and control concept of a DC/DC resonant converter in marine power systems. First, a mathematical model of the DC/DC resonant converter in the so-called CLLC topology is derived based on the generalized state-space averaging method. The model is used to design a dual-loop voltage control, which aims to regulate the voltage level at the low-voltage DC bus of the resonant converter. The dual-loop voltage control consists of the primal linear controller, which directly regulates the voltage and the reference generator, which dynamically modifies the voltage reference of the primal controller. The major advantage of the suggested control concept is the improved performance of the simple controller without the need to substitute it as well as the possibility to realize, if required, a multi-rate control concept. Simulation studies under different load conditions show that the suggested modeling and control concept improves voltage control and the closed-loop system response.

Keywords: Marine power systems, Resonant converter, Generalized average model, Reference generator, Model predictive control

1. INTRODUCTION

In order to meet the request for increased efficiency and flexibility, the power systems today are subject to significant infrastructural and operational changes. Some of these changes include increased penetration of renewable energy sources, installation of distributed storage systems, distributed electricity generation or the change of the communication and control architecture. When referring to the power networks in the marine systems, there is a notable interest to replace the existing AC grids with DC networks. As reported in Hansen et al. (2011), the onboard DC grids have series of advantages over AC grids such as fuel savings up to 20 %, more flexible placement of the electric components, improved overall dynamic response and reduced maintenance of the existing engines through more efficient operation. The major change in DC dominated marine power systems is that the frequency line transformers, which are required in AC grids, are replaced by the DC/DC converters. These converters are featured by high efficiency and power density and have a key role as interfacing components between different voltage levels. In particular, in the marine power systems, the resonant converters appear as favored technical solution among the DC/DC converters (Agamy et al. (2017)). Resonant converters come in different topologies and offer a series of practical advantages over conventional non-resonant topologies (like the dual active bridge). Some of these advantages include soft-switching of all switches, capability to operate at a very high switching frequencies, high efficiency and reduced electromagnetic interference.

1.1 Main Contribution

In contrast to the practical advantages the resonant converters offer and the popularity they gained, there are also challenges related to their control. To achieve the voltage control in the power converters, it is a common practice to apply linear control methods, like proportional-integral (PI) control, which assume a linear system representation. These methods are suitable for the fast execution (the sampling time of the converter controllers is in the range of several kHz) and easy to tune by practitioners. The direct application of the linear control methods is not possible in case of the resonant converters, due to the highly nonlinear nature of these power electronic components. For the PWM converters, like the buck-boost DC/DC converter, a simple, linear model is gained using the well-established state-space averaging method in Erickson and Maksimovic (2007). This method relies upon the assumption of small current ripple, which enables to represent the state variables in the model by their averaged values over the switching period, see Zhang et al. (2017). For the resonant converters, which operate at much higher frequencies than

PWM converters, this assumption is not valid. The modeling of resonant converters is more challenging due to the presence of two different system dynamics, i.e, dynamics of the DC and AC states respectively. The slower changing, DC states are related to the input and output capacitor of the converter, while the fast changing AC states refer to the currents and voltages of the so-called resonant network (see Fig. 1). The increased number of state variables in the mathematical model of the resonant converter simultaneously implies the need for an increased number of measurements to design a control concept. Apart from the modeling challenges, during controller design, we need to consider that these converters do not operate at a single switching frequency — thus, their performance is very sensitive to the selection of this frequency. Therefore, the analysis of the frequency range needs to be conducted first and the control scheme should enable the change of the switching frequency during simulation.

In this work, we consider a bidirectional DC/DC resonant converter for the application in the marine power systems and design a modeling and control concept to regulate the output voltage. This converter serves as an interfacing power electronic component between the high and the low voltage DC bus of the ship power system. We assume a number of DC loads to be connected in parallel to the low voltage DC bus. The DC loads might be turned on and off, changing thereby the total load power during operation. The control problem is to assure that the desired value of the output voltage is pertained and significant voltage drops are avoided in spite of the switching between different load levels. To stabilize the voltage and improve the dynamic response of the converter in closed loop, we design a model-based control concept.

First, we derive a mathematical model of the DC/DC converter in the so called CLLC topology (Jung et al. (2013), Zahid et al. (2015), Zou et al. (2019)), which is suitable for the controller design. Thereby, we apply the generalized state-space averaging method (Sanders et al. (1991)), which relies on the expansion of the periodic functions into Fourier series. To the best authors' knowledge, using this methodology, a control-oriented state-space model for the CLLC topology has not been suggested yet. Such approach facilitates the representation of the AC system dynamics, which are not negligible at the high switching frequencies of the CLLC converter. In the second step, we propose a control concept for the voltage control at the low voltage bus. The control concept assumes that a standard PI controller is applied to directly control the voltage at the low-voltage bus of the converter by adjusting the frequency. This frequency serves as an input to the frequency modulator which drives the converter internal half-bridges (H-bridges). Instead of replacing the PI controller with the more advanced one, like a model predictive controller (Maciejowski (2002), Bordons and Montero (2015), Kouro et al. (2015)), we pursue a more practical approach and design a double loop concept with an add-on scheme in the outer loop, which supports the primal controller in the inner loop. Such control concept design might be particularly useful in the power converter field, where the sampling frequencies are high and simple primal control approaches are preferred for hardware implementation. The resonant converter in our application can have a switching frequency of up to 20 kHz. As such, it is significant to reduce the complexity of the primal control algorithm and assure its fast execution. Furthermore, in some cases, the controller is already embedded, cannot be modified and we need to come up with a solution to improve the performance without replacing the existing controller. The main task of the add-on scheme, which exploits the idea of reference governors in Kolmanovsky et al. (2014), is to adapt the voltage reference of the PI controller by solving an unconstrained optimal control problem at each sampling time. The reference generator leverages the mathematical model of the CLLC resonant converter to form a closed-loop system model, to predict the time evolution of the closed-loop system and to use this prediction in the definition of the optimal control problem. The generated reference signal corresponds to an *artificial* reference which should ensure that the actual voltage reference value is reached (under certain performance criteria) for a broad range of load conditions. The adoption of the CLLC state-space model (with Fourier coefficients as AC states) for model-based reference generation has not yet been considered in previous works.

The paper is structured as follows. In Section 2 we introduce the CLLC topology, its properties and derive the characteristic curve for the frequency response amplitude. Section 3 derives the open-loop model of the CLLC converter. The control concept including the derivation of the closed-loop model and the reference generator design is presented in Section 4. In Section 5 simulation results are presented and discussed. Finally, Section 6 concludes and provides an outlook for future work.

2. BIDIRECTIONAL DC/DC RESONANT CONVERTER

2.1 Converter Topology

Fig. 1 shows the circuit topology of the bidirectional resonant converter applied in the middle voltage - low voltage (MV-LV) grid of the considered vessel system. The converter consists of two H-bridges and a resonant network which includes a high-frequency transformer. Thereby the primary bridge comprises the switches $Si1 - Si4$, while the switches of the secondary bridge include the components $So1 - So4$. Power switches of the primary bridge convert the power from DC to AC, while the secondary bridge has a rectifying role, converting the power from the AC back to the DC. The transformer T_r enables galvanic isolation between the primary and the secondary side. In our application, the transformer's turns ratio is defined as 1:1. Other components of the resonant network include resonant inductances L_{S1} and L_{S2}, transformer magnetizing inductance L_m and the resonant capacitors C_{S1} and C_{S2}. Since the resonant network is designed such that $L_{S1} = L_{S2}$ and $C_{S1} = C_{S2}$, it has a symmetric structure and the resulting converter is denoted as DC/DC converter in symmetric CLLC topology. With v_p and v_s, we denote the voltage at the input and output of the resonant network, respectively (with v_s being phase-shifted against v_p).

2.2 Equivalent Circuit Representation

When the load conditions change, the switching frequency f_s of the resonant converter might have to be adjusted in

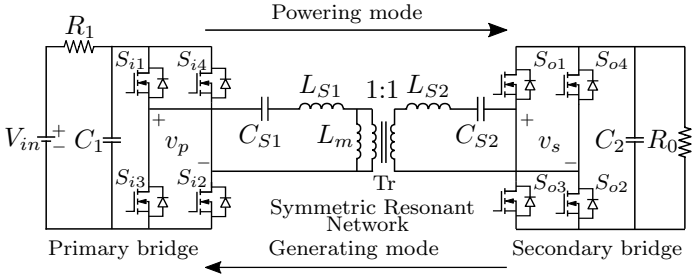

Fig. 1. Bidirectional full-bridge CLLC resonant converter.

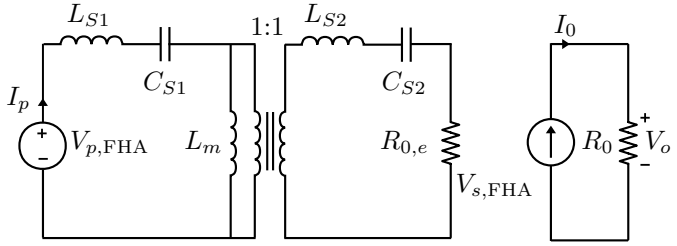

Fig. 2. Equivalent circuit of the CLLC converter.

order to maintain the requested voltage at the converter's output. We aim to keep the output voltage at 1 kV even when the load is changing from minimum to maximum power. To analyze the frequency range at which the CLLC converter should operate when the load is changing, we consider the equivalent circuit of the CLLC converter given in Fig 2. In the converter analysis, the equivalent circuit representation enables us to derive the transfer function for the resonant network by approximating the switching network of the primary and the secondary bridge using circuit elements, which describe their impact on the resonant intermediate network. In the equivalent circuit representation, the primary bridge can be modeled as an AC voltage source, while the secondary bridge can be modeled using an effective resistor of the value $R_{0,e}$. For more insight into these approximations, the interested reader is referred to Erickson and Maksimovic (2007).

2.3 Input-Output Gain Characteristic

The equivalent circuit representation facilitates to derive the input-output gain characteristic of the resonant network (i.e., from v_p to v_s) as a function of the switching frequency $\omega_s = 2\pi f_s$. As a first step, we define the following impedances:

$$Z_1(j\omega_s) = j\omega_s L_{S1} + \frac{1}{j\omega_s C_{S1}},\ Z_2(j\omega_s) = j\omega_s L_m, \quad (1)$$

$$Z_3(j\omega_s) = j\omega_s L_{S2} + \frac{1}{j\omega_s C_{S2}},\ Z_4(j\omega_s) = R_{0,e} \quad (2)$$

With the impedances (1)-(2), the forward frequency response of the resonant network, that is,

$$H_r(j\omega_s) = \frac{V_s(j\omega_s)}{V_p(j\omega_s)} \quad (3)$$

can be derived by transferring the impedances Z_3 and Z_4 from the secondary to the primary side of the transformer and by applying Kirchoff's 1st and 2nd law on the resulting resonant network circuit. This way, by expanding (3), the resulting frequency response can be summarized as:

$$H_r(j\omega_s) = \frac{Z_2\, Z_4}{Z_1\, Z_2 + Z_1\, Z_3 + Z_1\, Z_4 + Z_2\, Z_3 + Z_2\, Z_4} \quad (4)$$

where, for notational convenience, the dependence on $j\omega_s$ has been omitted. For the further analysis, it is common practice to express the frequency response (4) in terms of the characteristic parameters of the resonant converter. These are the first resonant frequency f_{r1}, the normalized frequency f_n, that is,

$$f_{r1} = \frac{1}{2\,\pi\,\sqrt{L\,C}},\ f_n = \frac{f_s}{f_{r1}}, \quad (5)$$

the second resonant frequency

$$f_{r2} = \frac{1}{2\,\pi\,\sqrt{(L+L_m)\,C}}, \quad (6)$$

the quality factor (providing an indication on the load size)

$$Q = \frac{Z_r}{R_{0,e}}, \quad (7)$$

with the converter impedance Z_r being defined as

$$Z_r = \frac{L}{C} \quad (8)$$

and the inductance ratio

$$k = \frac{L}{L_m}. \quad (9)$$

Due to symmetric structure of the resonant network, it holds $L = L_{S1} = L_{S2}$ and $C = C_{S1} = C_{S2}$. By exploiting (5)-(9) to substitute parameters in (4), we come up with a representation of $H_r(j\omega_s)$ that solely depends on f_n, k and Q. That said, we define the numerator $N(f_n)$ and denominator $D(f_n, k, Q)$ of $H_r(j\omega_s)$, i.e.,

$$N(f_n) = j\, f_n^3 \quad (10)$$

$$D(f_n,k,Q) = Q\,k + f_n\,k - 2\,Q\,f_n^4 - Q\,f_n^4\,k + j\,Q\,f_n^2 + j\,f_n^3\,k + j\,f_n^3 + j\,2\,Q\,f_n^2\,k \quad (11)$$

Eventually the resulting frequency response is given by

$$H_r(f_n,k,Q) = \frac{N(f_n)}{D(f_n,k,Q)}. \quad (12)$$

The DC/DC voltage gain characteristic follows from the amplitude of the frequency response (12):

$$|H_r(f_n,k,Q)| = \frac{f_n^3}{\sqrt{(D_{Re}(f_n,k,Q))^2 + (D_{Im}(f_n,k,Q))^2}} \quad (13)$$

$$\text{with}\quad D_{Re}(f_n,k,Q) = k\,(Q+f_n) - Q\,f_n^4\,(2+k),$$
$$D_{Im}(f_n,k,Q) = Q\,f_n^2\,(2\,k+1) + f_n^3\,(1+k).$$

The gain characteristics in Fig. 3 shows how the gain curve scales for different load values. By analyzing this characteristic we can determine the frequency range in which the converter should be operated for the given load variations such that the voltage at the output can be regulated to the desired value. Three frequency regions can be recognized from the gain curves: *Region 1* – the frequency region with frequencies below the second resonant frequency, i.e., $f < f_{r2}$, *Region 2* – between the first and the second resonant frequency, i.e., $f_{r2} \leq f \leq f_{r1}$ and *Region 3* – the one with frequencies above the first resonant frequency, i.e., $f > f_{r1}$. The converter is not operated in *Region 1* because the switches in the primary side suffer from significant losses.

To come up with the frequency region for our application, we recall that the designed converter should meet the voltage gain requirements in both directions of the energy

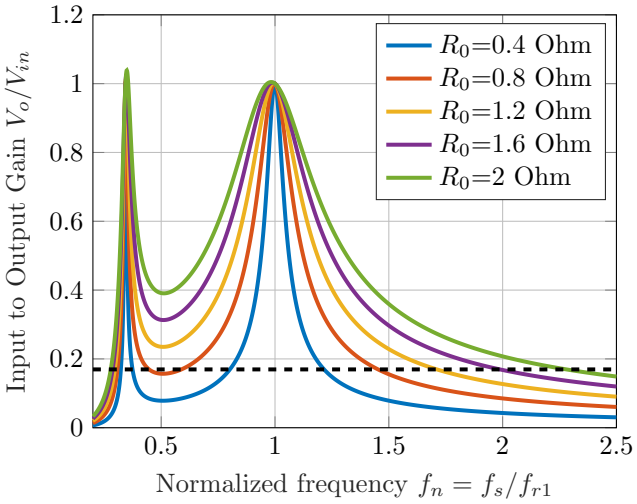

Fig. 3. Gain characteristic of the CLLC converter as a function of the load and the normalized frequency

flow. The high voltage DC bus connected to the converter's input has a level of $V_{in} = 5.9\,\text{kV}$, while the low voltage bus connected to the converter's output should remain at $V_o = 1\text{kV}$ for any load. Considering the powering mode, the gain of the converter should be equal to $V_o/V_{in} = 0.169$ which is represented by the dashed black line in Fig. 3. The minimum and maximum permitted load of the CLLC converter correspond to $P_{min} = 500$ kW and $P_{max} = 2.5$ MW, i.e, to the resistance values of $R_0 = 2\,\Omega$ and $R_0 = 0.4\,\Omega$ respectively. The gain of the converter is equal to the unity gain at the first resonant frequency f_{r1}. We already mentioned that the converter is never operated in *Region 1*. In *Region 2* the converter gain is lower than the unity gain, however the gain we seek cannot be reached for all load values. For this reason, Region 2 cannot be selected neither. For frequencies higher than f_{r1} the gain characteristic is monotonically decreasing and the gain of the converter is always less then one for any load in the considered range. The gain of 0.169 is achieved when the switching frequency is selected to be greater than f_{r1}. For a given load value the switching frequency is gained in the intersection of the horizontal gain line $V_o/V_{in} = 0.169$ and the gain characteristic for the corresponding load.

3. MODELING OF BIDIRECTIONAL DC/DC RESONANT CONVERTER

To model switched power converters, a range of methods has been applied including the state-space averaging methods, sample-data procedure, generalized state-space averaging method (see Mueller and Kimball (2018b)). The conventional state-space averaging method (Erickson and Maksimovic (2007)) requires an assumption of negligible current ripple. In this case, the state variables can be represented through its average component, i.e., only DC terms of Fourier series are sufficient to describe the dynamics of state variables. The assumption of a small ripple is not satisfied in case of resonant converters since the transformer current exhibits a pure AC nature.

3.1 Generalized State-Space Averaging

To derive a mathematical model of CLLC resonant converter, which can be used for control purposes, we apply a generalized state-space averaging method. The method has previously been used to derive a model of a dual active bridge (Qin and Kimball (2012), Mueller and Kimball (2018b), Mueller and Kimball (2018a)), but so far no applications for the CLLC topology have been suggested. The generalized averaging technique relies on the expansion of the periodic functions in the Fourier series and on using more terms of this series than only a DC term. In this way, a more accurate model is gained, but the order of the model increases.

In the generalized averaged approach, the state $x(t)$ is expanded in a Fourier series:

$$x(t) = \sum_{k=-\infty}^{k=\infty} \langle x \rangle_k(t)\, e^{j\,k\,\omega_s\,t} \tag{14}$$

where $\omega_s = 2\,\pi\,f_s$ and the complex number $\langle x \rangle_k$ is the k^{th} coefficient in the Fourier series which equals:

$$\begin{aligned} \langle x \rangle_k(t) &= \frac{1}{T}\int_{t-T}^{t} x(t)\, e^{-j\,k\,\omega_s\,t}\, dt \\ &= \frac{1}{T}\int_{t-T}^{t} x(t)\, \cos(k\,\omega_s\,t)\, dt \\ &\quad - j\,\frac{1}{T}\int_{t-T}^{t} x(t)\, \sin(k\,\omega_s\,t)\, dt \end{aligned} \tag{15}$$

In the following, a first harmonic approximation is used such that apart from the term $k = 0$ we include the terms $k = \pm 1$ to represent the state variables, while all other terms in the Fourier series are neglected. Every state of the system is thus approximated as follows:

$$\begin{aligned} x(t) &= \langle x \rangle_0(t) + \langle x \rangle_1(t)\, e^{j\,\omega_s\,t} + \langle x \rangle_{-1}(t)\, e^{-j\,\omega_s\,t} \\ &= \langle x \rangle_0 + 2\,\langle x \rangle_{1R}\, \cos(\omega_s\,t) - 2\,\langle x \rangle_{1I}\, \sin(\omega_s\,t) \end{aligned} \tag{16}$$

where x_{1R} and x_{1I} are the real and imaginary components of the first Fourier coefficient, respectively.

3.2 Open-Loop CLLC Model

To derive the nonlinear state-space model, let $s_1(d,\tau)$ and $s_2(d,\tau)$ denote the switching functions of the primary and the secondary bridge for the switching period T. The voltage at the output of the primary bridge v_p is then defined by:

$$v_p(\tau) = s_1(d,\tau)\, v_{in}(\tau) \tag{17}$$

while the voltage at the input of the secondary bridge equals:

$$v_s(\tau) = s_2(d,\tau)\, v_o(\tau) \tag{18}$$

where τ is the time within the switching period and d is the phase shift of the converter defined as a fraction of π, i.e., $d = \Phi/\pi \in [0,1]$ with Φ being the phase shift angle. The form of the switching functions s_1 and s_2 depends on the modulation strategy applied. For the single-phase shift modulation strategy (Mueller and Kimball (2018a)), considered in this work, the signals s_1 and s_2 are defined as:

$$s_1 = \begin{cases} 1, & 0 \le \tau \le \frac{T}{2} \\ -1, & \frac{T}{2} \le \tau \le T \end{cases} \tag{19}$$

$$s_2 = \begin{cases} 1, & \frac{d\,T}{2} \le \tau \le \frac{d\,T}{2} + \frac{T}{2} \\ -1, & 0 \le \tau \le \frac{T}{2} \text{ or } \frac{d\,T}{2} + \frac{T}{2} \le \tau \le T \end{cases} \tag{20}$$

We refer to the equivalent circuit representation given in Fig. 2 and introduce the following simplification. First,

we assume that the magnetizing inductance of the transformer L_m can be neglected. Second, the inductance L_{S2} and the capacitor C_{S2} on the transformer secondary side are referred to the primary side such that equivalent inductance L_{eq} and capacitance C_{eq} can be determined as a series connection of corresponding components, i.e.:

$$L_{eq} = L_{S1} + L_{S2} = 2\,L, \quad C_{eq} = \frac{C_{S1}\,C_{S2}}{C_{S1}+C_{S2}} = \frac{C}{2} \tag{21}$$

This representation simplifies the structure of the resonant network. By considering simplified circuit representations and by leveraging the definitions for v_p and v_s in (17)-(18) the following state space equations for the CLLC resonant converter are gained:

$$\dot{v}_{C_1} = -\frac{1}{C_1\,R_1}\,v_{C_1} - \frac{1}{C_1}\,s_1\,i_t + \frac{1}{C_1\,R_1}\,v_{in} \tag{22}$$

$$\dot{i}_t = -\frac{1}{L_{eq}} s_1\,v_{C_1} - \frac{1}{L_{eq}}\,v_{C_{eq}} - \frac{1}{L_{eq}}\,s_2\,v_o \tag{23}$$

$$\dot{v}_{C_{eq}} = -\frac{1}{C_{eq}}\,i_t \tag{24}$$

$$\dot{v}_0 = \frac{1}{C_2}\,s_2\,i_t - \frac{1}{C_2\,R_0}\,v_o \tag{25}$$

In this state-space representation, the input capacitor voltage v_{C_1}, the output capacitor voltage v_{C_2}, the transformer current i_t and the voltage across the equivalent capacitance $v_{C_{eq}}$ are identified as system states. Due to parallel connection, the output capacitor voltage equals the load voltage such that in the following we use $v_0 = v_{c_2}$.

We can now apply the generalized state-space averaging method on equations (22)-(25). As it follows from (16), every state of the CLLC converter model is a function of the DC average (zero-th Fourier coefficient), of the real and imaginary part of the 1st coefficient in the Fourier series. Therefore, each of these components represents an internal state in the full-order state-space model. The complete state vector can now be summarized as:

$$x_{OL} = \left[\bar{v}_{C_1},\ \bar{i}_t,\ \bar{v}_{C_{eq}},\ \bar{v}_o\right]^T \tag{26}$$

with the subvectors

$$\begin{aligned}
\bar{v}_{C_1} &= [\ \langle v_{C_1}\rangle_0,\ \ \langle v_{C_1}\rangle_{1R},\ \ \langle v_{C_1}\rangle_{1I}],\\
\bar{i}_t &= [\ \ \langle i_t\rangle_0,\ \ \ \langle i_t\rangle_{1R},\ \ \ \langle i_t\rangle_{1I}],\\
\bar{v}_{C_{eq}} &= [\langle v_{C_{eq}}\rangle_0,\ \langle v_{C_{eq}}\rangle_{1R},\ \langle v_{C_{eq}}\rangle_{1I}],\\
\bar{v}_o &= [\ \ \langle v_o\rangle_0,\ \ \ \langle v_o\rangle_{1R},\ \ \ \langle v_o\rangle_{1I}].
\end{aligned}$$

Simulative analysis of the full order model shows a potential for model reduction. The states in the model can be classified into DC states and AC states. The capacitors at the input and the output of the converter are such that the voltages across these elements can be represented by their average components. In a similar way, the internal states related to the resonant network, i.e., current i_t and voltage $v_{C_{eq}}$ have the pure AC nature with the average component equal to zero. For this reason, the state vector is reduced to:

$$x_{OL} = \left[\bar{v}_{C_1},\ \bar{i}_t,\ \bar{v}_{C_{eq}},\ \bar{v}_o\right]^T \tag{27}$$

with the subvectors

$$\begin{aligned}
\bar{v}_{C_1} &= \langle v_{C_1}\rangle_0, \quad \bar{i}_t = [\langle i_t\rangle_{1R},\ \ \langle i_t\rangle_{1I}],\\
\bar{v}_o &= \langle v_o\rangle_0, \quad \bar{v}_{C_{eq}} = [\langle v_{C_{eq}}\rangle_{1R},\ \langle v_{C_{eq}}\rangle_{1I}].
\end{aligned}$$

Applying the fundamental properties of the Fourier coefficients, as in Sanders et al. (1991), on the state vector (27), the generalized state-space averaging model is:

$$\dot{\langle v_{C_1}\rangle}_0 = -\frac{1}{C_1\,R_1}\,\langle v_{C_1}\rangle_0 + \frac{4}{C_1\,\pi}\,\langle i_t\rangle_{1I} + \frac{1}{C_1\,R_1}\,v_{in} \tag{28}$$

$$\dot{\langle i_t\rangle}_{1R} = -\frac{1}{L_{eq}}\,\langle v_{C_{eq}}\rangle_{1R} + \frac{2\sin(d\pi)}{L_{eq}\,\pi}\,\langle v_0\rangle_0 + \omega_s\,\langle i_t\rangle_{1I} \tag{29}$$

$$\dot{\langle i_t\rangle}_{1I} = -\frac{2}{L_{eq}\,\pi}\,\langle v_{C_1}\rangle_0 - \frac{1}{L_{eq}}\,\langle v_{C_{eq}}\rangle_{1I} + \frac{2\cos(d\pi)}{L_{eq}\,\pi}\,\langle v_0\rangle_0 - \omega_s\,\langle i_t\rangle_{1R} \tag{30}$$

$$\dot{\langle v_{C_{eq}}\rangle}_{1R} = \frac{1}{C_{eq}}\,\langle i_t\rangle_{1R} + \omega_s\,\langle v_{C_{eq}}\rangle_{1I} \tag{31}$$

$$\dot{\langle v_{C_{eq}}\rangle}_{1I} = \frac{1}{C_{eq}}\,\langle i_t\rangle_{1I} - \omega_s\,\langle v_{C_{eq}}\rangle_{1R} \tag{32}$$

$$\dot{\langle v_0\rangle}_0 = -\frac{1}{R_0\,C_2}\,\langle v_0\rangle_0 - \frac{4\sin(d\pi)}{\pi\,C_2}\,\langle i_t\rangle_{1R} - \frac{4\cos(d\pi)}{C_2\,\pi}\,\langle i_t\rangle_{1I} \tag{33}$$

The trigonometric terms in (28)-(33) follow from the application of the rules in Sanders et al. (1991) to the switching functions $s_1(t)$ and $s_2(t)$. For the Fourier coefficients of these signals it holds, see Qin and Kimball (2012):

$$\langle s_1\rangle_0 = \langle s_2\rangle_0 = 0 \tag{34}$$

$$\langle s_1\rangle_{1R} = 0, \qquad \langle s_1\rangle_{1I} = -\frac{2}{\pi} \tag{35}$$

$$\langle s_2\rangle_{1R} = \frac{-2\sin(d\pi)}{\pi}, \quad \langle s_2\rangle_{1I} = \frac{-2\cos(d\pi)}{\pi} \tag{36}$$

The state-space model (28)-(33) is a nonlinear model and therefore not appropriate for the voltage reference generator design which relies on the linear system representation. Thus, we linearize the model around the steady-state operating point. Lets assume that $\tilde{x}_{OL} = \tilde{x}_{OL} - X_0$, $\tilde{u}_{OL} = u_{OL} - U_0$ and $\tilde{y}_{OL} = y_{OL} - Y_0$ denote small signal perturbations for the state, control input and output variables around the steady-state vectors X_0, U_0 and Y_0, respectively. As control input, we use the switching frequency of the converter in radians, i.e., $u_{OL} = \omega_s$. The output voltage is selected as the controlled output, i.e., $y_{OL} = v_o$. After linearization around the steady-state, we gain the following open-loop model of the CLLC converter:

$$\dot{\tilde{x}}_{OL} = A_{OL}\,\tilde{x}_{OL} + B_{OL}\,\tilde{u}_{OL} \tag{37}$$

$$\tilde{y}_{OL} = C_{OL}\,\tilde{x}_{OL} + D_{OL}\,\tilde{u}_{OL} \tag{38}$$

with the system matrix A_{OL}, the input matrix B_{OL}, the output matrix C_{OL} and the feed-through matrix D_{OL}:

$$A_{OL} = \begin{bmatrix}
-\frac{1}{C_1\,R_1} & 0 & \frac{4}{C_1\,\pi} & 0 & 0 & 0\\
0 & 0 & \Omega_s & -\frac{1}{L_{eq}} & 0 & \frac{2\sin(D\pi)}{L_{eq}\,\pi}\\
-\frac{2}{L_{eq}\,\pi} & -\Omega_s & 0 & 0 & -\frac{1}{L_{eq}} & \frac{2\cos(D\pi)}{L_{eq}\,\pi}\\
0 & \frac{1}{C_{eq}} & 0 & 0 & \Omega_s & 0\\
0 & 0 & \frac{1}{C_{eq}} & -\Omega_s & 0 & 0\\
0 & -\frac{4\sin(D\pi)}{C_2\,\pi} & -\frac{4\cos(D\pi)}{C_2\,\pi} & 0 & 0 & -\frac{1}{C_2\,R_0}
\end{bmatrix},$$

$$B_{OL} = \begin{bmatrix} 0\\ I_{t,1I}\\ -I_{t,1R}\\ V_{C_{eq},1I}\\ -V_{C_{eq},1R}\\ 0 \end{bmatrix}, \quad C_{OL} = \begin{bmatrix}0&0&0&0&0&1\end{bmatrix}, \quad D_{OL} = 0 \tag{39}$$

where D, Ω_s, $I_{t,1R}$, $I_{t,1I}$, $V_{C_{eq},1R}$ and $V_{C_{eq},1I}$ are the respective steady-state values. Since the matrix A_{OL} is a function of the switching frequency in radians ω_s and the load R_0, the model of the CLLC converter resides to a group of parameter-varying models.

4. CONVERTER CONTROLLER DESIGN

With the open-loop model of the CLLC resonant converter, we propose the dual loop control concept, as shown in Fig. 4, to regulate the voltage at the low voltage bus of the DC/DC converter. The main idea is to improve the response of the closed loop system when the load power is changing and assure that the output voltage remains at 1 kV for all load conditions. The dual loop control concept leverages a simple, linear algorithm as a primal controller. This controller adjusts the switching frequency f_s, depending on the value of the control error, while the phase shift d is a function of f_s and the current load. In the outer loop, a voltage reference generator adjusts the *artificial* voltage reference v^A_{ref} of the primal controller to track the actual reference $v_{o,ref}$. To estimate the AC states, related to i_t and $v_{C_{eq}}$, we propose to utilize a harmonics estimator (not being subject of this paper) which relies on harmonic regression.

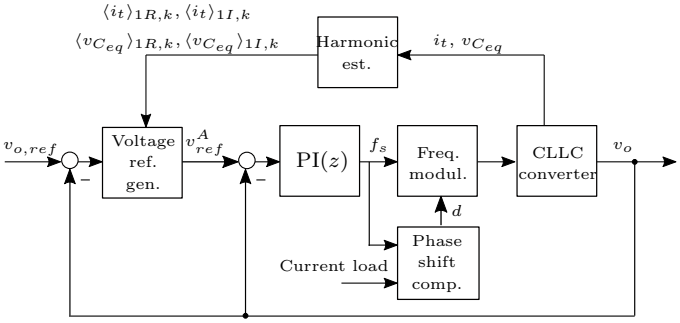

Fig. 4. Control architecture with reference generator and low level PI controller.

4.1 Closed-Loop CLLC Model

To design a voltage reference generator, a closed-loop system model must be known. The output voltage of the CLLC converter is controlled using the PI controller in the following digital realization:

$$u(k) = K_P\, e(k) + \gamma(k) \tag{40}$$
$$\gamma(k+1) = \gamma(k) + K_I\, T_s\, e(k) \tag{41}$$

where $e(k) = v^A_{ref}(k) - v_o(k)$ denotes the control error, v^A_{ref} the *artificial* reference value of the output voltage v_o, T_s is the controller sampling time, while $K_P > 0$ and $K_I > 0$ are the parameters of the PI controller. The integral term (41) has been discretized using forward-Euler discretization.

To form the closed-loop system model, the continuous state-space representation of the CLLC converter is discretized first assuming zero-order hold discretization such that we gain:

$$\tilde{x}_{OL}(k+1) = A_{OL,d}\,\tilde{x}_{OL}(k) + B_{OL,d}\,\tilde{u}_{OL}(k) \tag{42}$$
$$\tilde{y}_{OL}(k) = C_{OL,d}\,\tilde{x}_{OL}(k) \tag{43}$$

where $A_{OL,d}$, $B_{OL,d}$ and $C_{OL,d}$ are the discretized counterparts of the corresponding matrices in (39).

By inserting the control law (40)-(41) of the PI controller in the discretized system model (42)-(43) and augmenting the state vector with the additional state γ, representing the integrator state of the PI controller, we form a discrete-time state-space model of the closed-loop system:

$$\underbrace{\begin{bmatrix}\tilde{x}_{OL}(k+1)\\ \tilde{\gamma}(k+1)\end{bmatrix}}_{x_{CL}(k+1)} = A_{CL,d}\,\underbrace{\begin{bmatrix}\tilde{x}_{OL}(k)\\ \tilde{\gamma}(k)\end{bmatrix}}_{x_{CL}(k)} + B_{CL,d}\,\underbrace{\tilde{v}^A_{ref}(k)}_{u_{CL}(k)} \tag{44}$$
$$y_{CL}(k) = C_{CL,d}\,x_{CL}(k) \tag{45}$$

with

$$x_{CL} = \begin{bmatrix}\tilde{x}_{OL}\\ \tilde{\gamma}\end{bmatrix},\quad y_{CL} = \tilde{y}_{OL},\quad u_{CL}(k) = \tilde{v}^A_{ref} \tag{46}$$

$$A_{CL,d} = \begin{bmatrix}A_{OL,d} - K_P\, B_{OL,d}\,[0_{1\times 5}\ 1] & B_{OL,d}\\ [0_{1\times 5}\ 1] & 1\end{bmatrix} \tag{47}$$

$$B_{CL,d} = \begin{bmatrix}K_P\, B_{OL,d}\\ T_s\, K_I\end{bmatrix},\quad C_{CL,d} = [C_{OL,d}\ 0] \tag{48}$$

where $\tilde{\gamma} = \gamma - \gamma_0$ and $\tilde{v}^A_{ref} = v^A_{ref} - v_{o,ref}$ are the corresponding small-signal perturbations with respect to the operating point γ_0 and $v_{o,ref}$. This way, in the closed loop model, the deviation $\tilde{v}^A_{ref}$ from fixed reference $v_{o,ref}$ (that is, 1 kV) is the new control input.

Remark 1. The operating point (X_0, U_0, Y_0) of the closed-loop model refers to its steady state for $v_{o,ref} = 1\,\text{kV}$.

4.2 Reference Generation

Adopting the discrete-time state-space model of the closed-loop resonant converter, we can now design a scheme for the voltage reference generation. This scheme is based on the model predictive control concept in which the state-space model is utilized to predict the evolution of the closed-loop system dynamics over the time horizon of N_p time steps. The predictions are leveraged to define a finite-time optimal control problem which is solved at every time step. The number of time steps is selected, such that the prediction horizon equals at least the settling time τ_{set} of the closed-loop system, i.e., $\tau_{set} = N_p\, T_s$, where T_s denotes the sampling time of the reference generator. The formulation allows to run the reference generator at a different, lower frequency than the PI controller. In this way, a possibility is opened to further reduce the computational effort. To determine the voltage reference for the PI controller, the algorithm minimizes a quadratic cost function subject to the equality constraints that represent the closed-loop system dynamics, i.e.:

$$\begin{aligned}\min_{u_{CL,(\cdot|k)}} \sum_{i=1}^{N_p} Q\, \left\|(y_{CL,(k+i|k)} - y_{ref})\right\|_2^2 \\ + \sum_{i=0}^{N_u-1} R\, \left\|u_{CL,k+i|k}\right\|_2^2 \\ \text{s.t.}\quad x_{CL,k|k} = \hat{x}_{CL,k},\ (44), (45)\end{aligned} \tag{49}$$

In (49), the index $k+i\mid k$ denotes the prediction of the system output at time step $k+i$ starting from time step k, y_{ref} is the actual voltage reference that the system should maintain at the low voltage side (in our case 1000 V). The parameter $Q > 0$ represents the weighing of the output deviation at time step $k+i$, while $R > 0$ penalizes the magnitude of the control input. Upon solving the quadratic problem (49) at time k, the optimal sequence $u^\star_{CL,(\cdot|k)} = [u^\star_{CL,k|k}, \ldots, u^\star_{CL,k+N_u-1|k}]^T$ of voltage reference changes over the prediction horizon is gained. Only the first element is added to the steady-state value of $v_{o,ref} = 1000\,\text{V}$

and applied as a reference for the PI controller in the inner loop, i.e., $v^A_{ref,k} = v_{o,ref} + u^\star_{CL,k|k}$. By substituting the constraints into the cost, Problem (49) can be solved fast and the involved matrices even be pre-computed.

In the formulation of the optimization problem (49), the initial condition of the algorithm appears as an equality constraint. At each sampling time, i.e., at each run, the reference generator is initialized at the current state, $x_{CL,k|k}$. Consequently, the system states at time step k have to be either measured or estimated. The voltage at the input capacitance C_1 and the output capacitance C_2 (the DC states) are directly measured and thus $\langle v_{C_1}\rangle_0$, $\langle v_0\rangle_0$ are known at time k. The real and imaginary components of the current i_t and the voltage $v_{C_{eq}}$ (the AC states), though, have to be estimated as indicated at the beginning of the section. As measurements for the estimation, we assume that the current over the primary side inductance L_{S1} and the voltage across the primary side capacitor C_{S1} are available and perform the harmonic regression to determine $\langle i_t\rangle_{1R}$, $\langle i_t\rangle_{1I}$, $\langle v_{C_{eq}}\rangle_{1R}$ and $\langle v_{C_{eq}}\rangle_{1I}$ at time k.

5. SIMULATION RESULTS

5.1 Simulation Setup

The parameters of the considered CLLC resonant converter are listed in Table 1.

Table 1. Parameters of the CLLC converter.

Parameter	Value
Input voltage V_{in}	5900 V
Inductance L_{S1}, L_{S2}	40 μH
Inductance L_p	150 μH
Capacitance C_{S1}, C_{S2}	7.6 μF
Capacitance C_1, C_2	100 μF
Input resistance R_1	1 mΩ

The maximum load equals $P_{max} = 2.5\,\text{MW}$ ($R_0 = 0.4\,\Omega$), while the minimum load is $P_{min} = 500\,\text{kW}$ ($R_0 = 2\,\Omega$). To demonstrate the performance of the control concept, we consider the load changing sequence in Fig 5. The loads are denoted in terms of their resistance: $0.4\,\Omega$ corresponds to the largest load, $1\,\Omega$ to the medium load and $2\,\Omega$ stands for the smallest load. In our context the CLLC converter is a frequency modulated device. The frequency for the frequency modulation is set by the PI controller. The duty cycle for the frequency modulation is set to 50%. The phase shift d is changing depending on the load and the switching frequency. In our approach, it is determined according to calculus presented in Jung et al. (2013). For the PI controller and the voltage reference generator, the sampling frequencies are chosen to be equal. These sampling frequencies change based on the load conditions. For the largest load, the sampling frequency is 11 kHz, for the medium load 14.2 kHz, and for the maximum load 20.5 kHz. Since the discretized version of the PI controller is applied, with the change of the sampling frequency of the controller, the integral gain is changed as well (see (41)). This way, we realize a gain-scheduling PI controller, i.e., when the load changes, the parameters of the PI controller are adjusted accordingly and a more reasonable comparison with the dual-loop control concept can be made. The parameters of the reference generator are selected as follows: $N_p = 10$, $N_u = 10$, $Q = 5$, $R = 1$.

5.2 Simulation Results

To evaluate the simulation results, we use the following performance criteria (see Table 2): (i) min./max. LVDC voltage and the related overshoot/undershoot, (ii) root mean square error (RMSE) and (iii) the settling time for a 4% tolerance band around 1 kV. We particularly observe the output voltage at time steps when the load level is changing and compare the system response of standard with the dual-loop controller, designed in this contribution. When the load changes from the maximum to minimum or medium load, we obtain performance metrics which are almost equal for both control concepts (white columns in Table 2). Conversely, when changing from the minimum or medium to the maximum load (gray columns in Table 2), the dual loop concept outperforms the standalone PI controller noticeably.

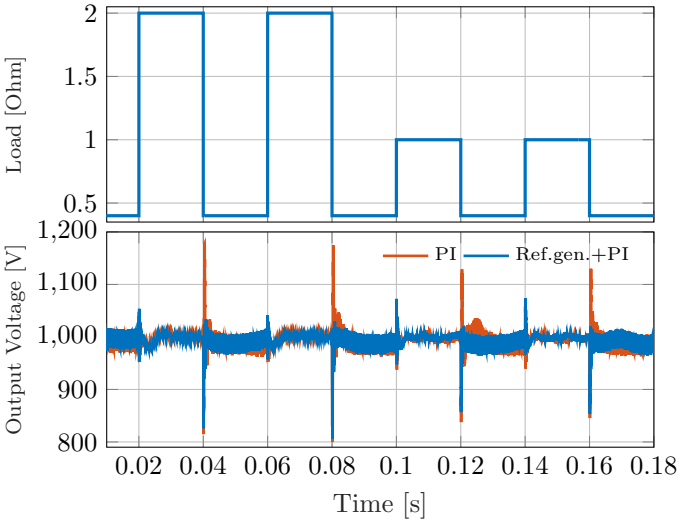

Fig. 5. Load sequence and the voltage at the LVDC bus.

To further analyze these benefits, we have selected two of these time intervals in Fig. 6 (A: min. to max. load; B: min. to medium load). Besides the output voltage, we illustrate the switching frequency, set by the PI controller, along with the phase shift. For time interval A, the dual loop control scheme is able to reduce the voltage overshoot by 12.7% from 1185.7 V to 1035.1 V, the RMSE by 34.3% and the settling time by 51.1%. The initial undershoot, when switching the load, cannot be avoided as it can not be anticipated by the reference generator. Further, we note that the dual loop controller counteracts the predicted over-/undershoot in voltage by adjusting the reference for the PI controller (green solid line) in the opposite direction. Time interval B enforces this observation, showing a 9.3% reduced overshoot, a 27.6% smaller RMSE and a 53.8% reduced settling time. Similar improvement can be recognized for the other corresponding time intervals. In conclusion, we note that the dual loop control concept outperforms the gain-scheduling PI controller and enable to dynamically adapt to excessive load changes.

6. CONCLUSION

We have proposed a modeling and voltage control concept for a DC/DC resonant converter, applied in marine power systems. Leveraging a generalized state-space averaging method, we have presented a control-oriented model of

Table 2. Overview of performance measures during respective load change intervals.

Load Change [Ω]	0.4 → 2.0	2.0 → 0.4	0.4 → 2.0	2.0 → 0.4	0.4 → 1.0	1.0 → 0.4	0.4 → 1.0	1.0 → 0.4
Time interval [s]	0.02–0.04	0.04–0.06	0.06–0.08	0.08–0.1	0.10–0.12	0.12–0.14	0.14–0.16	0.16–0.18
Ref. gen. + PI								
Vmin [V]	953	812.1	952.4	805.7	947.7	855.3	960.5	846.1
Vmax [V]	1057	1035.1	1053.7	1031.3	1078.3	1023.7	1079.8	1022.2
RMSE [V]	14.6517	41.863	16.366	37.294	18.846	30,240	18.527	31.374
Settling Time [s] (4%)	0.00021	0.00065	0.00012	0.00064	0.00030	0.00060	0.00020	0.00070
PI								
Vmin [V]	950.9	811.9	941.5	794.7	932.9	837.8	929.5	845.5
Vmax [V]	1048.1	1185.7	1034.3	1175.1	1071.3	1129.2	1071.5	1134.0
RMSE [V]	14.276	63.747	18.378	53.047	17.256	41.786	17.264	39.762
Settling Time [s] (4%)	0.00025	0.00133	0.00042	0.00122	0.00040	0.00130	0.00050	0.00100

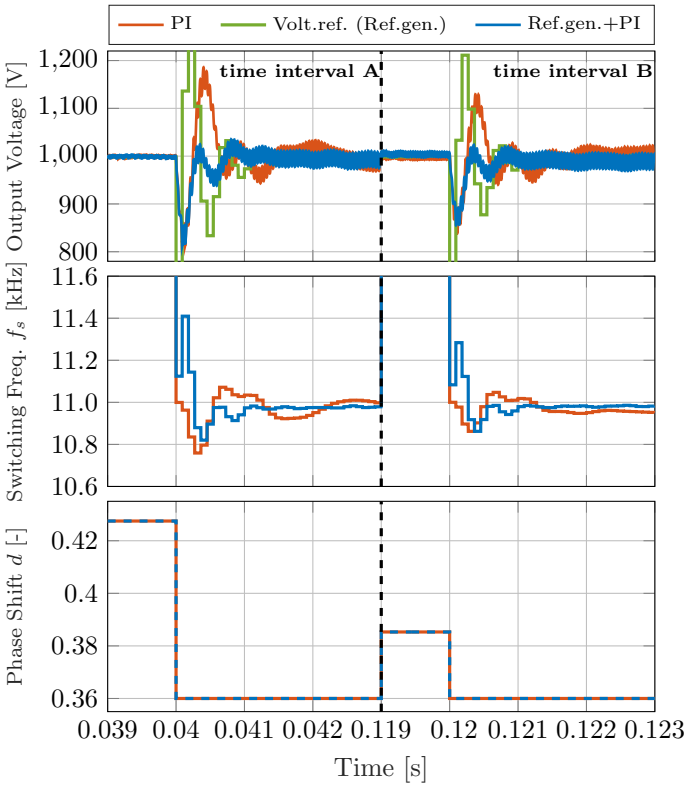

Fig. 6. Controlled output (voltage), voltage reference from ref. generator, control input (switching frequency) and the feedforward term (phase shift).

the resonant converter in the CLLC topology. A linearized version of the model is used to design a dual loop control scheme to regulate the voltage at the low voltage DC side. The dual loop scheme relies on a primal PI controller, which is complemented by a voltage reference generator. A simulation study demonstrates its ability to improve the dynamic system response and to stabilize the voltage when the load is changing. As part of future work, we will examine how the controlled CLLC converter performs (under disturbances elsewhere in the system) when connected to the remaining vessel power system which involves further power converters and local controllers.

REFERENCES

Agamy, M.S., Dong, D., Garcs, L.J., Zhang, Y., Dame, M.E., Wu, X., and Pan, Y. (2017). A high power medium voltage resonant dual active bridge for MVDC ship power networks. *IEEE Journal of Emerging and Selected Topics in Power Electronics*, 5(1), 88–99.

Bordons, C. and Montero, C. (2015). Basic principles of MPC for power converters: Bridging the gap between theory and practice. *IEEE Industrial Electronics Magazine*, 9(3), 31–43.

Erickson, R.W. and Maksimovic, D. (2007). *Fundamentals of power electronics*. Springer Science & Business Media.

Hansen, J.F., Lindtjorn, J.O., and Vanska, K.O. (2011). Onboard DC grid for enhanced DP operation in ships.

Jung, J., Kim, H., Ryu, M., and Baek, J. (2013). Design methodology of bidirectional CLLC resonant converter for high-frequency isolation of DC distribution systems. *IEEE Trans. on Power Electronics*, 28(4), 1741–1755.

Kolmanovsky, I., Garone, E., and Di Cairano, S. (2014). Reference and command governors: A tutorial on their theory and automotive applications. In *2014 American Control Conference*, 226–241.

Kouro, S., Perez, M.A., Rodriguez, J., Llor, A.M., and Young, H.A. (2015). Model predictive control: MPC's role in the evolution of power electronics. *IEEE Industrial Electronics Magazine*, 9(4), 8–21.

Maciejowski, J.M. (2002). *Predictive control: with constraints*. Pearson education.

Mueller, J.A. and Kimball, J.W. (2018a). An improved generalized average model of DC–DC dual active bridge converters. *IEEE Transactions on Power Electronics*, 33(11), 9975–9988.

Mueller, J.A. and Kimball, J.W. (2018b). Modeling dual active bridge converters in DC distribution systems. *IEEE Trans. on Power Electronics*, 34(6), 5867–5879.

Qin, H. and Kimball, J.W. (2012). Generalized average modeling of dual active bridge DCDC converter. *IEEE Transactions on Power Electronics*, 27(4), 2078–2084.

Sanders, S.R., Noworolski, J.M., Liu, X.Z., and Verghese, G.C. (1991). Generalized averaging method for power conversion circuits. *IEEE Transactions on Power Electronics*, 6(2), 251–259.

Zahid, Z.U., Dalala, Z.M., Chen, R., Chen, B., and Lai, J. (2015). Design of bidirectional DC-DC resonant converter for vehicle-to-grid (V2G) applications. *IEEE Trans. on Transportation Electrification*, 1(3), 232–244.

Zhang, K., Shan, Z., and Jatskevich, J. (2017). Large- and small-signal average-value modeling of dual-active-bridge dcdc converter considering power losses. *IEEE Transactions on Power Electronics*, 32(3), 1964–1974.

Zou, S., Mallik, A., Lu, J., and Khaligh, A. (2019). Sliding mode control scheme for a CLLC resonant converter. *IEEE Transactions on Power Electronics*, 34(12), 12274–12284.